

Asymmetric microstrip line feed multimode cylindrical dielectric resonator antenna

O. G. AVADANEI¹, M.G. BANCIU^{2,*}, L. NEDELCU², M. AVADANEI³

¹Alexandru Ioan Cuza University, Iasi, Romania

²National Institute of Materials Physics, Atomistilor 405A, 077125 Magurele, Romania

³Petru Poni Institute of Macromolecular Chemistry, Iasi, Romania

The aim of this work is the development of a cylindrical dielectric resonator antenna with multimodal operation. In order to use modes with different radiation patterns, the field distributions were investigated. Using a feeding solution with the resonator placed asymmetrically above a wide microstrip feeding line, we managed to excite and identify 17 operating modes in the 1.8-4.5 GHz frequency band. In dissimilarity with the symmetric configuration, the proposed feeding allows excitation of new modes, which exhibit a magnetic dipole radiation pattern. The new added modes enhance the antenna pattern diversity and increase the antenna capacity to mitigate the multipath effects.

(Received January 12, 2022; accepted August 10, 2022)

Keywords: Dielectric resonator antennas, Microwaves, High order modes

1. Introduction

Dielectric resonator antennas exhibit such interesting features as: high radiation efficiency, low frequency variation with temperature, no conductor losses, small size, small weight, and low profile.

The microstrip feeding system was already used by different authors [1-3], but the effects of the asymmetrical positioning of the dielectric resonator antenna (DRA) above the microstrip feeding line and the modes, which can be excited by such a geometry were not studied before, to the best of our knowledge.

DRA's with different shapes are suitable for higher mode operation [4-10]. However, here, we investigate only cylindrical DRA. In a previous work, we identified higher modes excited in a high permittivity cylindrical DRA excited by a central rectangular slot in the ground plane [11]. The wide variety of modes that could be excited in the resonator, make the DRA suitable for multi or wide band applications, which are of a constant interest today [12-13]. Additionally different modes could provide different radiation patterns.

We expect that different feed configurations would excite different modes, however, present literature doesn't provide information about the modes that will be excited with different feeding systems, or about their radiation performances and their radiation patterns. The aim of our paper is to identify the operating modes of a DRA placed asymmetrically on the microstrip feeding line, to study their radiating performances and to present their radiating patterns. Full wave electromagnetic simulations are performed by using Ansys HFSS software.

2. Antenna configuration

The measurements and simulations were made for a cylindrical dielectric resonator antenna, with the diameter $\varnothing = 18.2$ mm, and height $h = 10.8$ mm, placed asymmetrically above a 4.6 mm wide microstrip line on a Rogers 5880 substrate as presented in Fig. 1. A high dielectric permittivity of $\epsilon_r = 86.5$ was used for both simulation and measurements. The dielectric resonator was set on the Rogers substrate with a 50 μm thick layer of low dielectric loss glue. The substrate dimensions were 62 mm in length, 50 mm in width, and 1.57 mm in thickness.

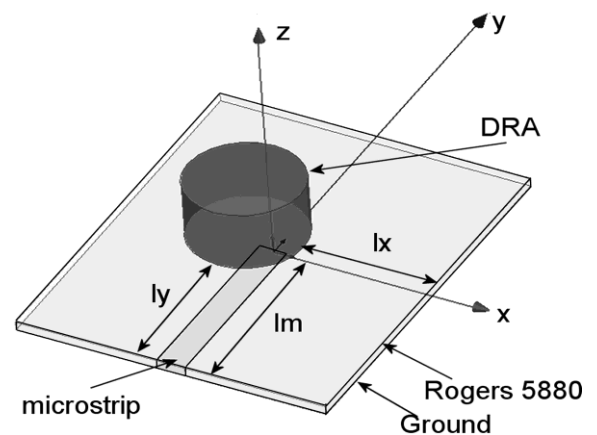


Fig. 1 Antenna geometry

The microstrip line length was $l_m = 31$ mm, and the resonator position is given by: $l_x = 21.3$ mm and $l_y = 24.4$ mm. This position was chosen because it provides the largest number of excited modes. The aim of the paper was to identify and study as many modes as possible, however

a good impedance match for all those mode was not possible. The dielectric resonator material is $\text{Ba}_{0.5}\text{Pb}_{0.5}\text{Nd}_2\text{Ti}_5\text{O}_{14}$ (BNT), a Pb doped Barium Neodymium Titanate ($\text{Ba}_{1-x}\text{Pb}_x\text{Nd}_2\text{Ti}_5\text{O}_{14}$) ceramic. The material preparation is described in [14], and its dielectric parameters were measured using the Hakki-Coleman method [15].

3. Results

The antenna reflection coefficient, was measured using an Agilent E8361A network analyzer in an anechoic chamber and compared with the simulated values as shown in Fig.2. From the measured data, shown in Fig. 2a, it is clear that, in this configuration, the antenna presents a lot of S_{11} deeps corresponding to different modes and our goal was to identify them. However, to obtain a good impedance match for all these resonances, it is impossible in practice and therefore we assign a resonance even to small S_{11} deeps.

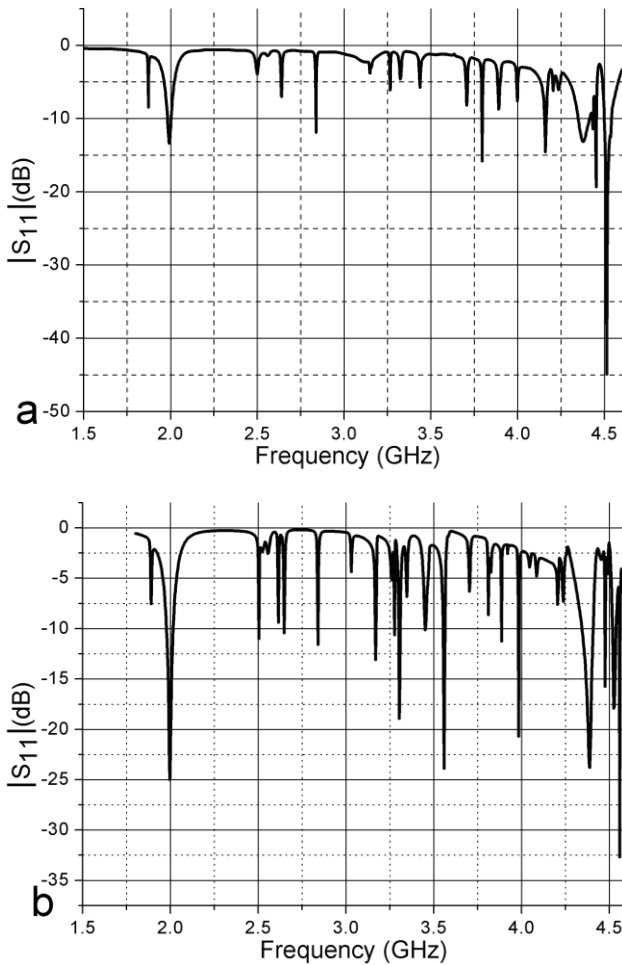


Fig. 2 Reflection coefficient of the DRA (a) measured, (b) simulated

At present, there are two analytical theories about cylindrical DRA. The first theory considers all the DRA walls as perfect magnetic walls. The second theory was

developed by Long [17] and assumes perfect magnetic boundary conditions on all the DRA walls except for the bottom DRA base, which is treated as an electric wall boundary condition. The resonant frequencies of the transverse electric (TE) and the transverse magnetic (TM) modes in the first model are given by relations (1) and (2) [16], and in the Long model by relations (3) and (4) [17].

$$f_{r\text{TE}_{nmp}} = \frac{1}{2\pi\sqrt{\epsilon_0\mu_0\epsilon_r}} \left[\left(\frac{\rho_{nm}}{a} \right)^2 + \left(\frac{p\pi}{h} \right)^2 \right]^{1/2} \quad (1)$$

$$f_{r\text{TM}_{nmp}} = \frac{1}{2\pi\sqrt{\epsilon_0\mu_0\epsilon_r}} \left[\left(\frac{\rho'_{nm}}{a} \right)^2 + \left(\frac{p\pi}{h} \right)^2 \right]^{1/2} \quad (2)$$

$$f_{r\text{TE}_{mnp}} = \frac{1}{2\pi\sqrt{\epsilon_0\mu_0\epsilon_r}} \left[\left(\frac{\rho_{nm}}{a} \right)^2 + \left(\frac{(2p+1)\pi}{2h} \right)^2 \right]^{1/2} \quad (3)$$

$$f_{r\text{TM}_{mnp}} = \frac{1}{2\pi\sqrt{\epsilon_0\mu_0\epsilon_r}} \left[\left(\frac{\rho'_{nm}}{a} \right)^2 + \left(\frac{(2p+1)\pi}{2h} \right)^2 \right]^{1/2} \quad (4)$$

where a is the radius of the resonator, h is the height, and ρ_{nm} and ρ'_{nm} are the solutions of the Bessel functions $J_n(k_\lambda a)$ and $J'_n(k_\lambda a)$, respectively. For each mode, n , m and p are the radial, azimuthal and axial index, respectively.

For each mode, we will investigate three resonance frequencies: the resonance frequency in the measured S_{11} data of the antenna, the resonance frequency in the simulated S_{11} of the antenna and the computed frequency given by one equation from (1) to (4).

Some modes correspond to the first theoretical model and others to the second model. However, in practice, neither of these two models could explain all the modes that appear in the antenna. The reason for this is that the resonator sits partially on the microstrip line and partially on dielectric substrate. Therefore, the boundary condition on the bottom base of the cylindrical DRA is neither an electric wall nor a magnetic wall.

In order to evaluate the radiation performance of the modes, we also measured the antenna radiation patterns for all the resonances. The radiation patterns were measured in an anechoic chamber, with an Agilent E8361A network analyzer and a wide band WBH 1-18 GHz corrugated horn antenna from Q-Par as receiver, and the results are presented in Figs. 3 and 4.

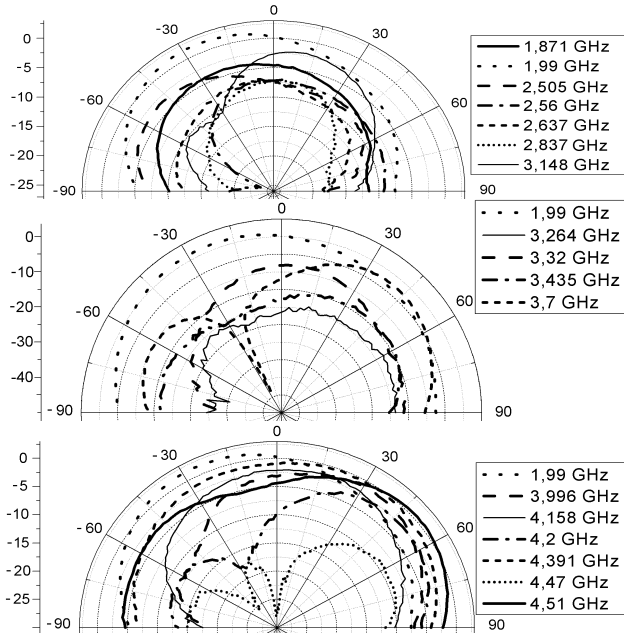


Fig. 3 Measured radiation patterns E_θ in $\varphi = 0$ plane

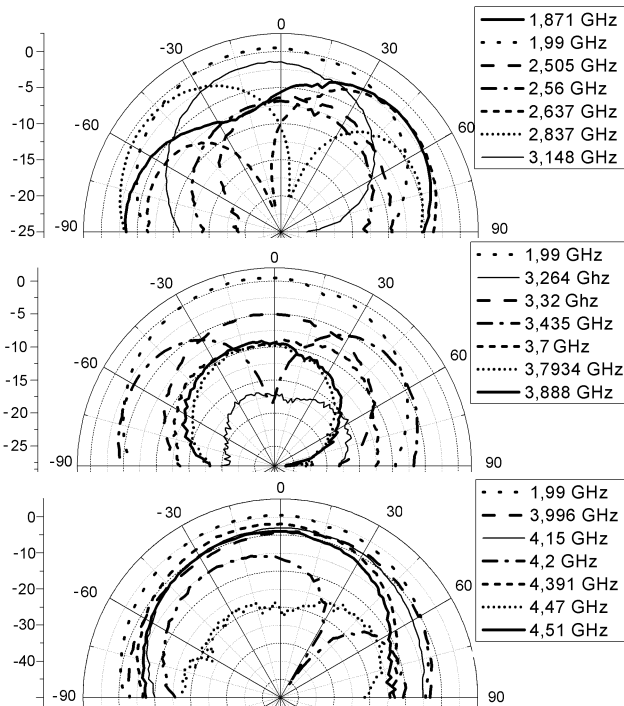


Fig. 4 Measured radiation patterns E_φ in $\varphi = 90^\circ$ plane

The angles θ and φ are standard spherical coordinates. All radiation patterns are normalized to the gain of the fundamental mode, $HEM_{11\delta}$ with the resonant frequency of 1.99 GHz, for $\varphi = 0$ and $\theta = 0$.

One of the most interesting features of this antenna is the fact that the first resonance, which appeared at 1.871 GHz in measurements and 1.889 GHz in simulations does not correspond to the fundamental $HEM_{11\delta}$ mode as in the case of an isolated resonator. The radiation patterns show a poor performance of this mode for E_θ , and E_φ presents a minimum around the axis. This pattern is similar to the

radiation pattern of a magnetic dipole antenna. Moreover, the field distributions obtained in HFSS simulations, and presented in Fig. 5, show a rotational symmetry of the electric field in resonator, which explains the measured radiation pattern. This field distribution could correspond to the TE_{010} or to the TE_{me010} modes. The only difference between these two modes is the fact that, for the TE_{010} mode, the resonant frequency is independent on the resonator height. Our simulations showed that the resonant frequency of this mode depends on the resonator height proving that the 1.871 GHz resonance corresponds to the TE_{me010} mode with the computed resonant frequency of 1.547 GHz according to (3).

The second resonance, which was found at 1.99 GHz in measurements, was assigned to the $HEM_{11\delta}$ mode according to the field configuration obtained in simulation at 1.995 GHz. The third measured resonance was spotted at 2.505 GHz in measurements and simulations. The field configuration corresponds to the TE_{me110} mode, already identified in [9], with the theoretical frequency of 2.28 GHz computed using (3). However, the theoretical frequency of the TE_{111} mode, which was calculated at 2.625 GHz by using (1), is closer to the measured frequency.

The next resonance was found at 2.56 GHz in measurements and at 2.555 GHz in simulations. The field distribution presented in Fig. 6 show a rotational structure of magnetic field in the xy plane, and two rotational structure of electric field in the xz plane, which correspond to the TM_{011} mode, with the theoretical frequency of 2.625GHz calculated using (2).

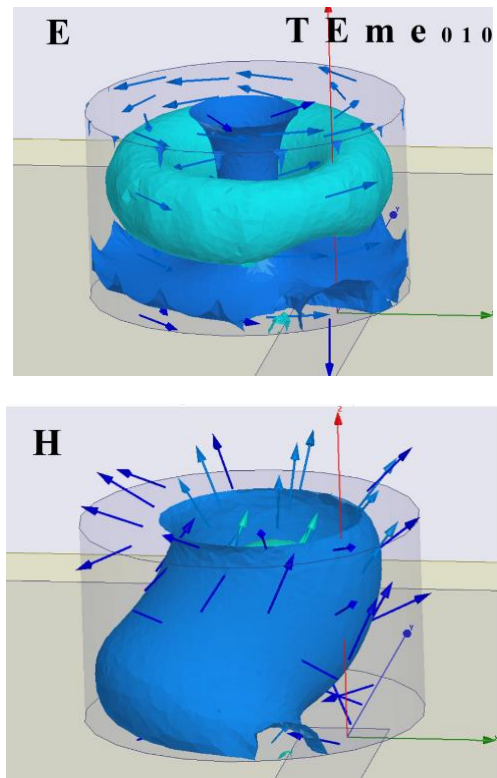


Fig. 5. Field distributions at 1.871 GHz (color online)

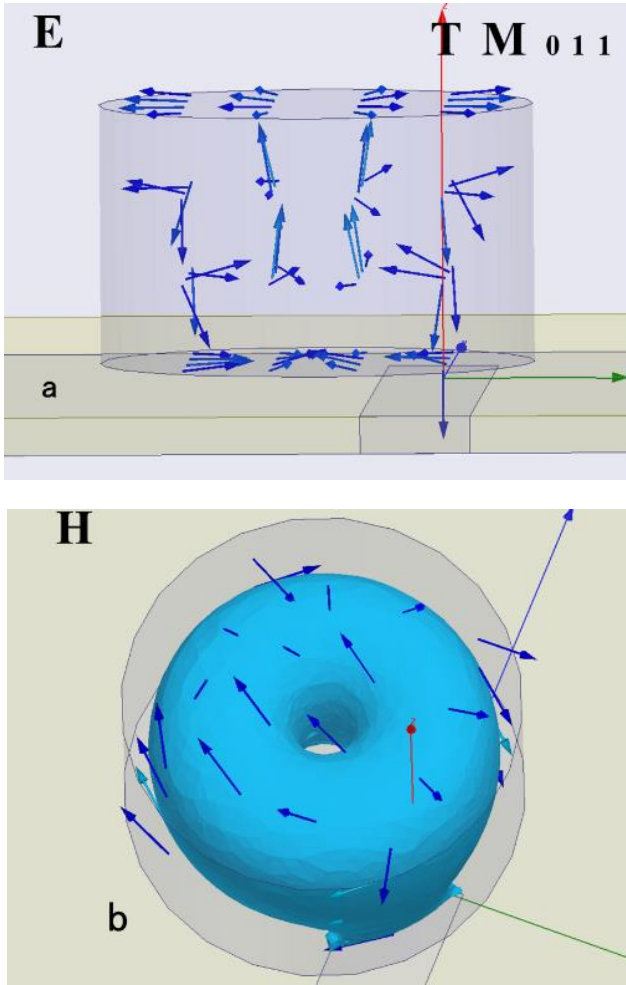


Fig. 6. Field distributions at 2.56 GHz: (a) electric; (b) magnetic (color online)

The measured S_{11} data show a resonance at 2.637 GHz. The simulations on this mode give a resonant frequency of 2.648 GHz and field distributions, which are displayed in Fig. 7. The field patterns exhibit four maxima of electric and magnetic field, and the electric field lines are mainly oriented along z axis, suggesting that this is the TM_{211} mode. However because the electric field lines between two maxima should close above the microstrip line, the mode is actually the $TMme_{211}$ mode with the resonant frequency of 2.824 GHz computed using (4).

This mode cannot be obtained with a symmetrical excitation solution, and, from Fig. 7, we can see that the electric field lines, at the top of the resonator, in the left side and close view have an opposite orientation comparative to the electric field lines in the right side and far view. This structure is somehow similar to a rotational electric field structure, which can explain the magnetic dipole characteristic found for $E\varphi$ at 2.637 GHz in measurements.

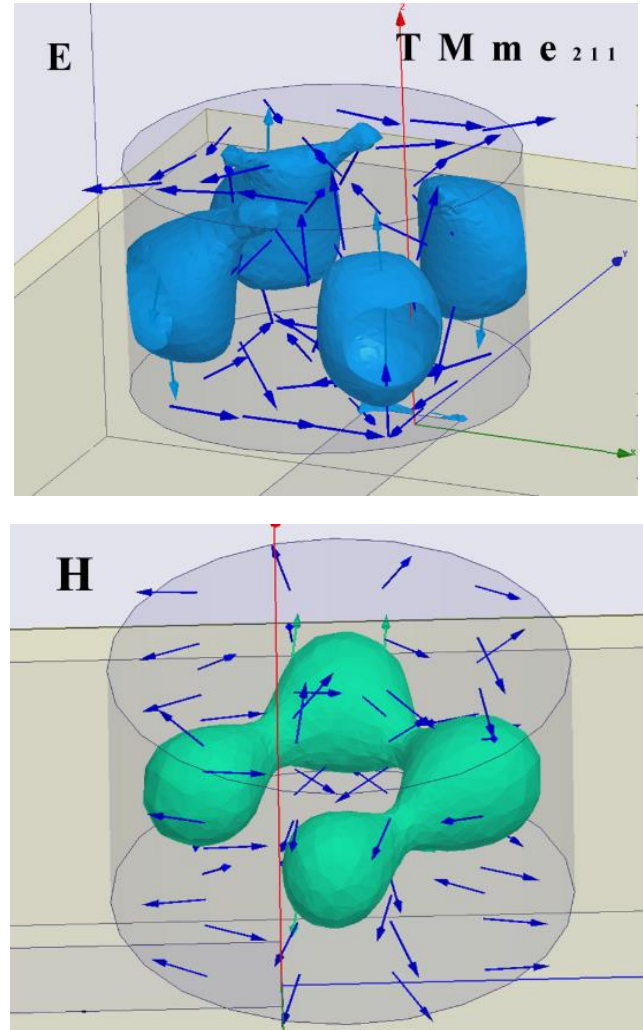


Fig. 7. Field distributions at 2.637 GHz (color online)

The measured 2.837 GHz resonance corresponds to the mode simulated at 2.84 GHz. The field distribution (Fig. 8) reveals two superposed rotational structures of electric field rotating in the opposite directions, which resemble to a TE_{011} mode. However, the resonant frequency of the TE_{011} mode calculated using (1) is as low as 2.016 GHz and the only explanation why this mode appears at such a higher frequency is that the microstrip line changes the boundary conditions and this is in fact the $TEme_{011}$ mode. This mode is another mode that can be excited only with an asymmetric feeding and has a radiation pattern of a magnetic dipole as can be seen in Fig. 4.

The measured resonance at 3.148 GHz was assigned to the mode for which the simulated field distributions are displayed in Fig. 9. The simulated resonance frequency of this mode is 3.168 GHz. The field configuration shows two layers of magnetic field situated between three layers of electric field, which corresponds to the HEM_{112} mode. The particular case of the HEM_{112} mode, the TM_{112} , has the theoretical frequency of 3.159 GHz calculated using (2). The radiation pattern show that this mode has good radiation performances, close to that of the fundamental mode.

Another measured resonance, but with poor radiation performances, was found at 3.264 GHz. It was assigned to the 3.275 GHz resonance from simulations, and its field configuration corresponds to the TM_{me311} mode with the resonant frequency of 3.258 GHz computed using (4).

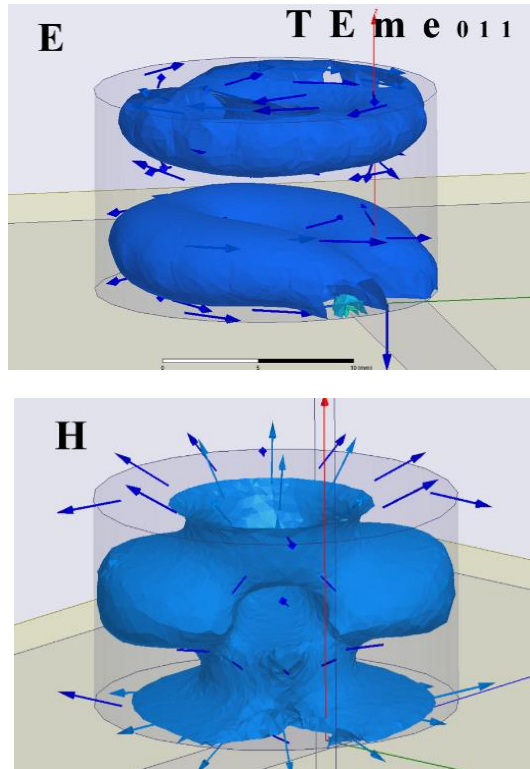


Fig. 8. Field distributions at 2.837 GHz (color online)

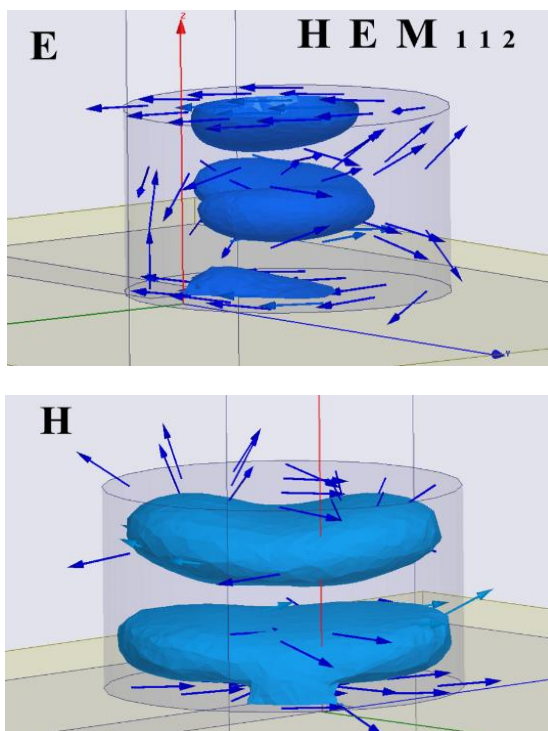


Fig. 9 Field distributions at 3.148 GHz (color online)

The next resonance was spotted in measurements at 3.32 GHz. At the same frequency, the simulations revealed the configuration displayed in Fig. 10; with three maxima of magnetic field situated between four maxima of electric field on radial direction. The magnetic field lines are chiefly perpendicular on z axis meaning that this configuration definitely corresponds to the TM_{121} mode with the 3.35 GHz frequency computed by (2). Figs. 3-4 show that this mode has one of the best radiation performances, almost similar to the fundamental mode, and we could not excite it with a symmetrical feeding.

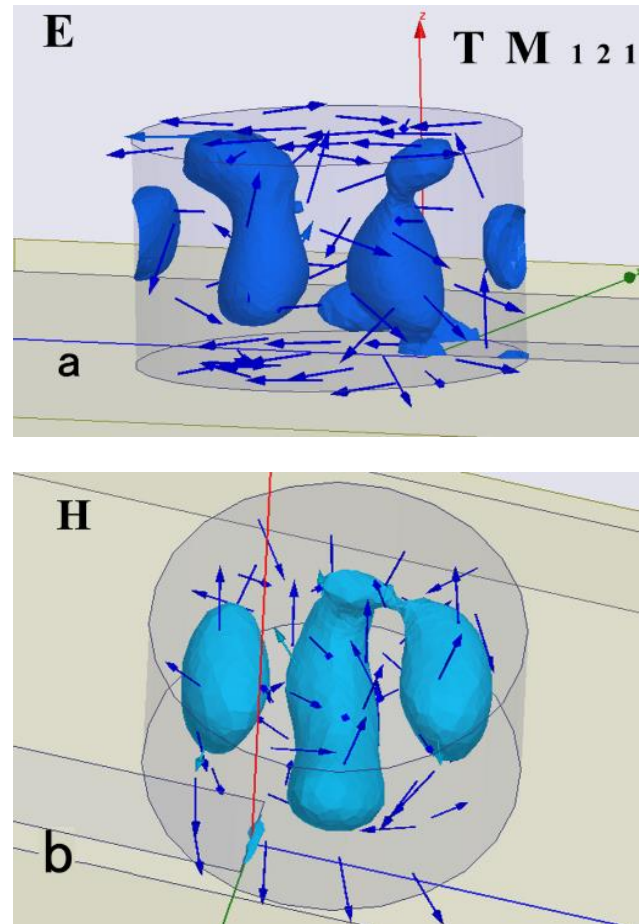


Fig.10 Field distributions at 3.32 GHz (color online)

The resonance at 3.435 GHz in measured S_{11} data correspond to the resonance at 3.45 GHz obtained in simulations. The field patterns obtained in simulations and presented in Fig. 11 reveal two concentric rotational structures of electric field and three magnetic field maxima situated in center and between the two rotational structures of electric field. This configuration is a slightly distorted version of the TE_{me020} mode, although the resonant frequency of the TE_{021} mode (3.451 GHz) is closer to the measured resonance. Fig. 4 reveals that this mode has magnetic dipole radiation pattern, which confirms our identification. This is another mode, which cannot be excited with a symmetric feeding.

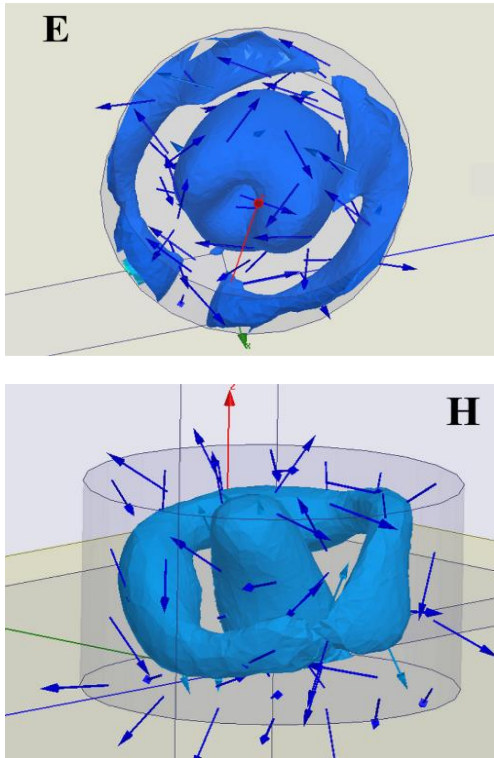


Fig. 11. Field distributions at 3.435 GHz for the TE_{me020} mode (color online)

At 3.7 GHz we found another resonance in both measurements and simulations. The field distributions displayed in Fig. 12 show magnetic field oriented mostly perpendicular to the z axis suggesting that this is a TM mode. There are two layers of four magnetic fields so $n = 2$, $m = 1$ and $p = 2$. Consequently this is the TM_{212} mode with the theoretical frequency of 3.45 GHz computed using (2).

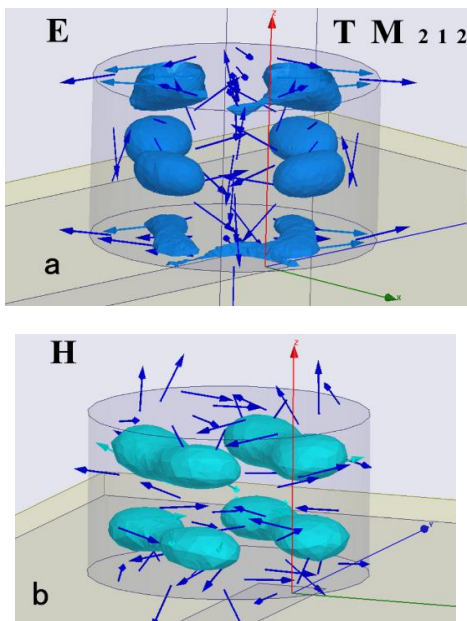


Fig. 12. Field distributions at 3.7 GHz (color online)

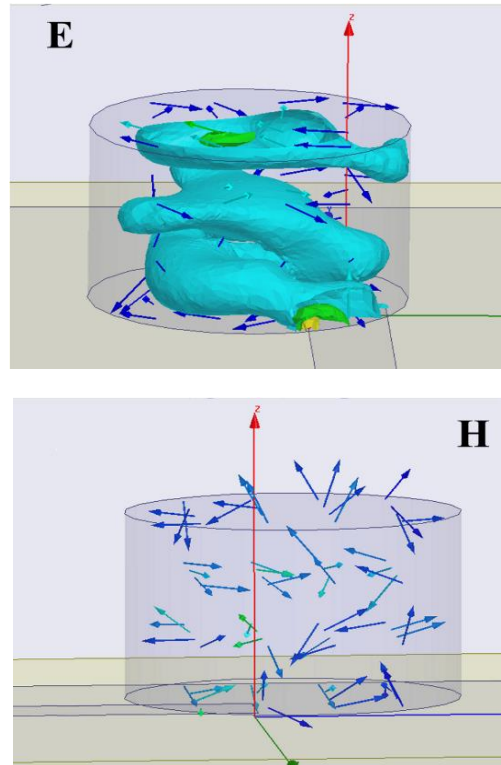


Fig. 13. Field distributions at 3.996 GHz for the TE_{me012} mode (color online)

The next measured resonance was discovered at 3.7934 GHz, which corresponds in simulations to the resonance at 3.81 GHz. The field distribution show six maxima of electric and magnetic field and the magnetic field lines are chiefly oriented along the z axis. Consequently, this is the TE_{me310} mode with the frequency of 3.66 GHz, although the TE_{311} mode with the 3.894 GHz frequency according (1) is closer to the measured frequency. This mode has very poor radiation performances.

The next identified measured resonance was found at 3.996 GHz and the most nearby resonance in simulations was at 3.985 GHz. The field distribution is displayed in Fig. 13 and reveals three structures of rotating electric field situated one above the other, which suggest that this is the TE_{me012} mode with the resonant frequency of 3.969 GHz calculated from (3).

At 4.158 GHz, the measured antenna has a resonance with one of the best radiating performances. The field distribution, obtained in HFSS simulations at this frequency, is displayed in Fig. 14 and shows two central and four smaller lateral electric field maxima. The magnetic field on z axis present three loops, which corresponds to a TE_{me112} mode, with the theoretical frequency of 4.311 GHz computed from (3). The strong and continuous maxima of the electric field on the top of the resonator explains the very good radiating performances of this mode.

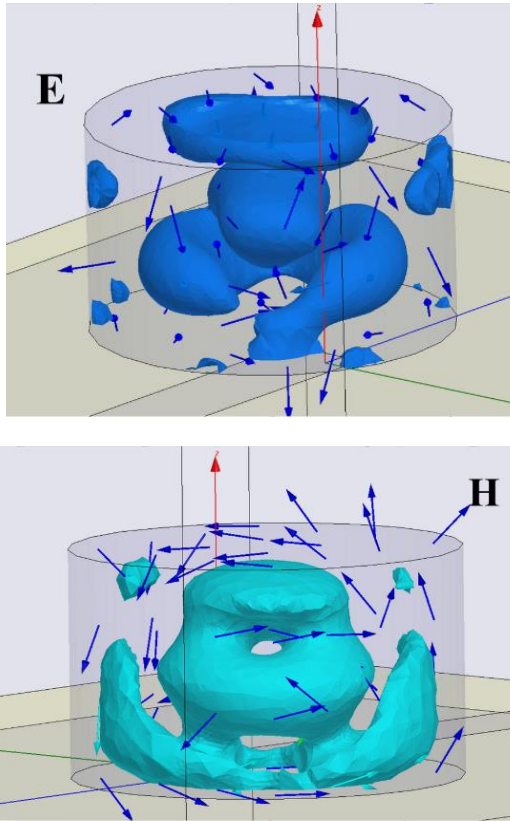


Fig. 14. Field distributions at 4.158 GHz for the TE_{me121} mode (color online)

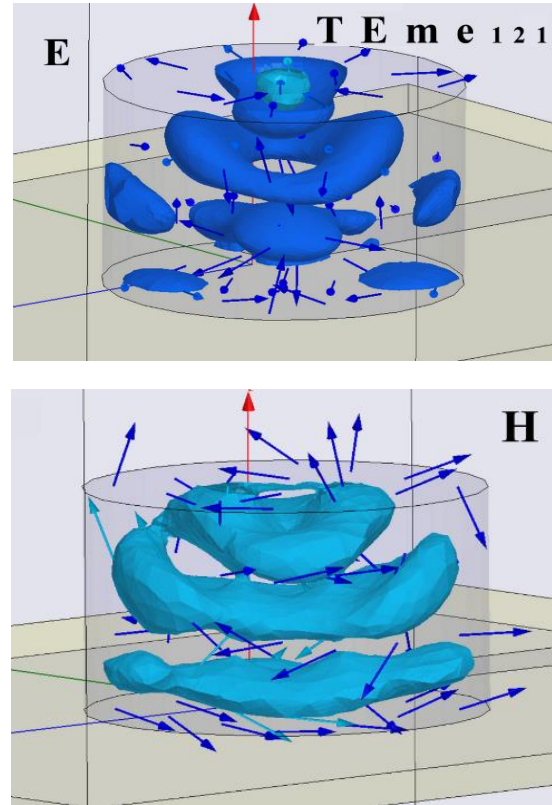


Fig. 16 Field distributions at 4.385 GHz (color online)

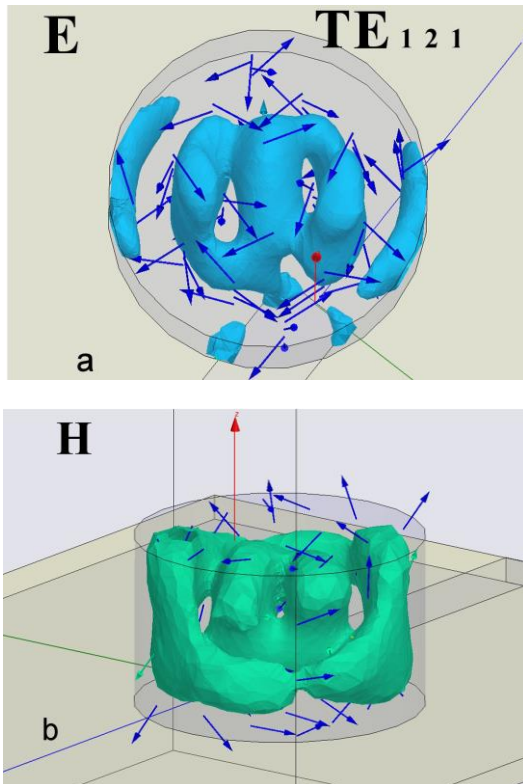


Fig. 15 Field distributions at 4.2 GHz (color online)

The 4.2 GHz S_{11} resonance discovered in measurements was assigned to the 4.238 GHz resonance obtained in simulations. The field patterns inside the resonator presented in Fig. 15 exhibit four maxima of the magnetic field situated between five electric field maxima on radial direction, which correspond probably to the TE_{121} mode with the 4.227 GHz theoretical frequency resonance.

The next pair of resonances were spotted at 4.391 GHz on measurements and 4.385 GHz in simulations. The field distribution presented in Fig. 16 could correspond to a TE_{me112} mode or a TE_{12p} mode. Still, Fig. 16b shows in the upper part three rotational structures of magnetic field, which could appear only for a TE_{12p} mode, and the fact that there are another field distribution in the lower part means that this is the TE_{me121} mode with the frequency of 4.54 GHz computed using (3). The field distributions displayed in Fig. 16 explain the good radiating performances of this mode observed in figures 4.

Using the field configuration obtained in simulations for the 4.475 GHz resonance, the measured 4.47 GHz resonance was associated to be TE_{me411} mode with the computed resonant frequency of 4.34 GHz. Again, the resonance frequency of the TE_{411} mode 4.53 GHz is closer to the measured resonance.

4. Conclusions

The asymmetric feeding method is able to excite a large number of modes. In this case we managed to

identify 17 operating modes. All radiating modes available with a symmetric feeding are also excited with the proposed asymmetric feed, and, in both configurations, antenna presents two wide bands characteristic between 3.9 GHz and 4.165 GHz, and another between 4.26GHz and 4.445 GHz. The $TE_{m_{112}}$ mode is responsible for the first band and the $TE_{m_{121}}$ mode for the second band.

Moreover, this solution enabled the excitation of six new modes: $TE_{m_{010}}$, $TM_{m_{211}}$, $TE_{m_{011}}$, TM_{121} , $TE_{m_{020}}$, and $TE_{m_{012}}$, all with good radiation performances, and with the exception of the $TM_{m_{211}}$ and TM_{121} modes, all modes present radiation pattern more or less similar to a magnetic dipole antenna. The asymmetric feeding solution is better than the symmetrical feeding because it enables the excitation of more modes, meaning more operation frequencies, and because it could provide modes with electric dipole and modes with magnetic dipole radiation pattern. This ability could be useful in wireless communications in order to mitigate the fading effects, because an antenna with different radiation patterns could provide different transmission routes and offer a better communication channel.

One of the most interesting features of this antenna is the fact that it can operate at a frequency below the frequency of the fundamental HEM_{116} mode. This capability is offered by the $TE_{m_{010}}$ mode, which we managed to excite only with the proposed feeding configuration.

Consequently, the proposed feeding solution has no drawback comparative to the symmetric solution, but it gives to the antenna new operating frequencies, and offers the capability to modify the antenna radiation pattern only by changing the operation mode. Using the existing models, with the equations (1), (2), (3) and (4), and knowing the possible modes, identified in this paper, one can predict the operating frequencies, and the radiation pattern, which can be obtained at these frequencies for a cylindrical DRA feed asymmetrically by a microstrip line.

Acknowledgements

This research was funded by a grant of Ministry of Research and Innovation, CNCS - UEFISCDI, project number PN-III-P2-2.1-PED-2019-3351 and Core Program PN19-03 (contract no. 21 N/08.02.2019).

References

- [1] R. A. Kranenburg, S. A. Long, *Electron. Lett.* **24**(18), 1156 (1988).
- [2] O. G. Avadanei, M. G. Banciu, L. Nedelcu, *IEEE Antennas Wirel. Propag. Lett.* **13**, 1585 (2014).
- [3] M. Ene-Dobre, M. G. Banciu, L. Nedelcu, G. Stoica, C. Busuioc, H. V. Alexandru, *J. Optoelectron. Adv. M.* **13**(10), 1298 (2011).
- [4] Bin Li, K. W. Leung, *IEEE Trans. Antennas Propag.*, **53**(7), 2200 (2005).
- [5] Laila K. Hady, D. Kajfez, A. A. Kishk, *IEEE Trans. Antennas Propag.* **57**(5), 1328 (2009).
- [6] T. H. Chang, J. F. Kiang, *IEEE Trans. Antennas Propag.* **57**(10), 3316 (2009).
- [7] X. S. Fang, K. W. Leung, *IEEE Trans. Antennas Propag.* **59**(6), 2409 (2011).
- [8] L. K. Hady, D. Kajfez, A. A. Kishk, *IEEE Trans. Microw. Theory Tech.* **56**(12), 3079 (2008).
- [9] Y-M. Pan, K. W. Leung, K.-M. Luk, *IEEE Trans. Antennas and Propagation* **59**(8), 2780 (2011).
- [10] C.-H. Li and T.-Y. Chiu, *IEEE Trans. Terahertz Science and Technology* **7**(3), 284 (2017).
- [11] O. G. Avădănei, G. M. Banciu, I. Nicolaescu, L. Nedelcu, *IEEE Trans. Antennas Propag.* **60**(11), 5032 (2012).
- [12] T. A. Denidni, Z. Weng, *IET Microw. Antennas Propag.* **5**(4), 450 (2011).
- [13] H. H. B. Rocha, F. N. A. Freire, R. S. T. M. Sohn, M. G. da Silva, M. R. P. Santos, C. C. M. Junqueira, T. Cordaro, A. S. B. Sombra, *IET Microw. Antennas Propag.* **2**(6), 580 (2008).
- [14] A. Ioachim, M. I. Toacsan, M. G. Banciu, L. Nedelcu, H. Alexandru, C. Berbecaru, D. Ghetu, G. Stoica, *Mater. Sci. Eng. B*, **109**(1-3), 183 (2004).
- [15] B. W. Hakki, P. D. Coleman, *IRE Trans. Microw. Theory Techn.* **MTT-8**(4), 402 (1960).
- [16] D. K. Cheng, *Field and Wave Electromagnetism*, Ch. 9, Addison Wesley, 1989.
- [17] S. A. Long, M. W. McAllister, L. C. Shen, *IEEE Trans. Antennas Propag.* **31**(3), 406 (1983).

*Corresponding author: gbanciu@infim.ro